Melting in single screw extruders

A. L. Halmos, J. R. A. Pearson and R. Trottnow
Department of Chemical Engineering & Chemical Technology, Imperial College, London SW7 2AZ, UK
(Received November 1976; revised 3 February 1978)

A model for the melting of granules in a single screw extruder is presented in Part I. It is consistent with observations of earlier workers and retains some of the ideas introduced by Tadmor in his model; however, it assumes that the solid bed of granules cannot stand large differences of principal stresses and so account has to be taken explicitly of the downstream force balance on the solid bed and in the melt pool. Detailed quasi-analytic results are given for a Newtonian (constant viscosity) fluid in Part II. These illustrate the model for a particularly simple case and have relevance for some materials. A more elaborate numerical scheme is described in Part III for a non-Newtonian model and results are presented for comparison with the predictions of other theories and with experiments.

Part III: Solutions for a power law temperature-dependent viscous melt

INTRODUCTION

Over the past 7 years several workers have combined to develop a large computer program for predicting the melting process in a single screw extruder. Part I of this paper described the underlying mathematical model for a general non-Newtonian melt using the lubrication approximation and a power law viscosity with exponential temperature dependence.

In this part of the paper we shall describe the computational scheme, give some results for a typical solution and make some comments on the applicability of numerical calculations for prediction purposes.

BASIC EQUATIONS

The 6 zone* model used for the numerical calculations is fully described in Part I. A resumé of the equations used in the iterative numerical solution scheme is given below for convenience. These can be compared with those used in Part 2, where greater simplifications were made. A brief description of the numerical scheme itself is given in Appendix 1.

We use much of the notation of Parts I and II, with the geometry of *Figure 1b*. (Note however that the sign of the z-coordinate is different and that zones D and E have been exchanged. This does not lead to any complications or difficulties in that zones D and E are always taken together.) The relevant equations are (Part I, Shapiro, Halmos and Pearson[3]):

overall mass balance:

$$\rho_s M_{Ax} + \rho_m (M_{Bx} + M_{Cx} + M_{Dx} + M_{Ex}) = M_T \qquad (1)$$

force balance on zone A:

$$-\bar{H} Z \frac{dp}{dx} = S_{ABx} + S_{ACx} + S_{ADx} + S_{AEx} \qquad (2)$$

with $\bar{H} = H - \hat{\delta}_C - \delta_D$ where $\hat{\delta}_C$ is an average depth of zone C.

The melting rate is given by:

$$\frac{dM_{Ax}}{dx} = -(R_C + R_D + R_E + R_B) \qquad (3)$$

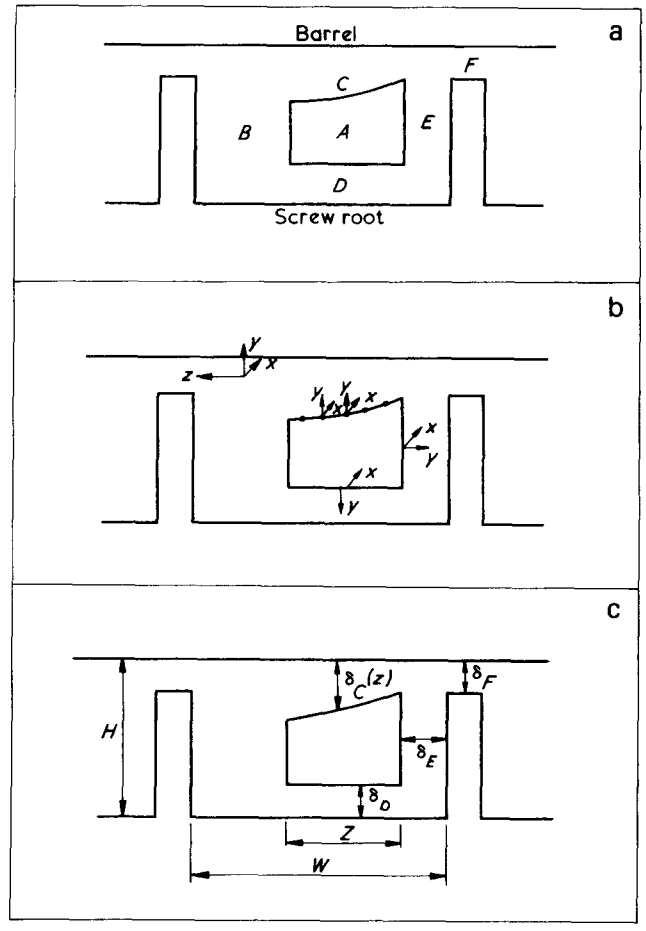

Figure 1 Screw geometry: (a) *A*, solid bed of polymer granules: *B*, melt pool; *C*, barrel/solid bed interface; *D*, screw root/solid bed interface; *E*, screw flight/solid bed interface; *F*, leakage over the flight; (b) note the different use of y in the analysis of zones

* For convenience only, we have introduced the leakage over the flight as a sixth zone (see *Figure 1a*).

0032–3861/78/101199–18$02.00

The average velocity of the solid bed is:

$$v_{Ax} = M_{Ax}/\overline{H}Z \tag{4}$$

As reasoned in Part I, we shall neglect S_{ABx} and R_B, though in principle S_{ABx} could be included from the solution given by equation (6) below. We shall thus assume that the melt pool (zone B) is fed only by molten material swept into it from the upper layer, i.e. zone C. We then have:

$$\frac{dM_{Bx}}{dx} = m_{Cz} - m_{Fz} \tag{5}$$

which is equal to the melting rate in zone C, R_C. The mass flow rate M_{Bx} obeys a relation depending on several variables:

$$M_{Bx} = f(W - Z - \delta_E,\ v_{Ax},\ \frac{dp}{dx},\ H,\ v_{bx},\ v_{bz},\ \mu)$$

where f is a function given here by the Rowell and Finlayson model for a viscous flow in a box with moving sides (see Shapiro[2] or Part II, Shapiro, Halmos and Pearson[3]). Thus:

$$f = \overline{W}^2\left(Av_{bx} - B\frac{\overline{W}^2}{\mu}\frac{dp}{dx}\right) + \frac{8v_{Ax}H}{\pi^3}\sum_{n-1}^{\infty}\frac{\tanh\frac{n\pi\overline{W}}{2H}}{n^3} \tag{6}$$

where:

$$A = \frac{8}{\pi}\sum_{n=1}^{\infty}\frac{\tanh\frac{n\pi H}{2\overline{W}}}{n^3}$$

$$B = \frac{H}{12\overline{W}} - \frac{16}{\pi^5}\sum_{n=1}^{\infty}\frac{\tanh\frac{n\pi H}{2\overline{W}}}{n^3}$$

$$\overline{W} = W - Z - \delta_E$$

Here the constant value for the viscosity, μ, was calculated from:

$$\mu = C_0 e^{-b(\overline{T}-T_0)}(I_2)^{-s} \tag{7}$$

where I_2 is the second invariant of an assumed mean value of the rate of deformation tensor given by:

$$I_2 = \frac{1}{4}\left[\left(\frac{v_{bx}}{H}\right)^2 + \left(\frac{v_{bz}}{H}\right)^2 + \left(\frac{v_{Ax}}{W - Z - \delta_E}\right)^2\right] \tag{8}$$

and $\overline{T}$ is a velocity-weighted average temperature of the melt flowing into zone B from zone C, given by:

$$\overline{T} = \frac{\int_0^{\delta_C(z)} v_{Cz}(y)T(y)dy}{\int_0^{\delta_C(z)} v_{Cz}(y)dy} \quad \text{at } z = Z \tag{9}$$

As in Part II, we assume that the density of the polymer in zone A is equal to ρ_s and in all other zones equal to ρ_m. We shall also assume that the densities of melt and solid, the specific heat of melt and solid, C_m and C_s, and the thermal conductivities, k_m and k_s, are separately constant. It would be possible, though, to make them functions of the temperature and of the isotropic pressure and so vary with position. However, it is not believed that such additional complexity is demanded at this stage.

The calculations can be carried out for a tapered or untapered screw. We shall assume that the screw is tapered when discussing the typical solution below.

A major part of the program is concerned with calculating expressions for R_C, R_D, R_E, S_{ACx}, S_{ADx} and S_{AEx}, and we shall now describe the processes involved in analysing zones C, D and E, starting with zone C. Before doing so, it is necessary to calculate the leakage over the flight in the region called zone F. Since the calculations are identical with those leading to the mass flow rate in the z-direction at any given point in zone C, they will be discussed simultaneously noting where necessary any difference in boundary conditions.

The stress equilibrium equations (i.e. equations 11 and 12 in Part I) are:

$$\frac{\partial p}{\partial x} = \frac{\partial}{\partial y}\left(\mu\frac{\partial v_{Cx}}{\partial y}\right) \tag{10a}$$

$$\frac{\partial p}{\partial z} = \frac{\partial}{\partial y}\left(\mu\frac{\partial v_{Cz}}{\partial y}\right) \tag{10b}$$

where μ is given by equation (7), I_2 being suitably defined.

Neglecting the convective terms in the energy balance (this follows from a small Graetz number approximation, Part I, equation 18a) we obtain:

$$k_m\frac{\partial^2 T}{\partial y^2} = -4\mu I_2 \tag{11}$$

Labelling the integration constants that arise in a first integration of equations (10a) and (10b) ψ_1 and ψ_2 we have:

$$\psi_1 = \frac{\int_0^{\delta_C(z)}\frac{y}{\mu}\frac{dp}{dx}dy - v_{bx} + v_{Ax}}{\int_0^{\delta_C(z)}\frac{1}{\mu}dy} \tag{12a}$$

$$\psi_2 = \frac{v_{bz}}{\int_0^{\delta_C(z)} \frac{1}{\mu}\,dy} \tag{12b}$$

Here we assume that dp/dx is known and a function of x only (see equation 2). Furthermore, we use the drag flow assumption (see Part I) in zone C, so that the stress field in zone A is dominated by the isotropic component of the pressure. Hence equation (10b) reduces to:

$$\frac{\partial(\mu \partial v_{Cz}/\partial y)}{\partial y} = 0$$

v_{bx} and v_{bz} are the boundary conditions for v_{Cx} and v_{Cz} at $y = \delta_C(z)$.

In zone F, ψ_1 and ψ_2 are given by equation (12) with δ_F replacing $\delta_C(z)$, where $\partial p/\partial z$ is taken to be:

$$\frac{\partial p}{\partial z} = \frac{\partial p}{\partial x}\frac{\pi D_b}{\cos\beta W_f}$$

This is a good approximation since we can assume dp/dx to be a slowly varying function of x and the pressure to be linearly distributed over the flight (see Shapiro[2]).

A predictive–corrective method is used by solving the above equations (i.e. equation 10 and the equation for $\partial p/\partial z$). When convergence is reached, we obtain the mass flow rate in the z-direction in zone C as:

$$m_{Cz}(z) = v_{bz}\frac{\int_0^{\delta_C(z)}\left\{\int_0^{y}\frac{dy'}{\mu}\right\}dy'}{\int_0^{\delta_C(z)}\frac{dy}{\mu}} \tag{13}$$

and the mass flow rate over the flight as:

$$m_{Fz} = m_{Cz}(z=0) = \int_0^{\delta_F}\left\{\int_0^{y}\frac{dy'}{\mu}\left(\frac{dp}{dz}y' + v_{bz}\Big/\int_0^{\delta_F}\frac{dy''}{\mu}\right)\right\}dy \tag{14}$$

From these equations we calculate $\delta_C(z)$ for any given point z. The only difference between zone C and zone F calculations is that the boundary conditions at $y = 0$ are different. Thus, we have in zone C:

$$v_{Cx} = v_{Ax},\ v_{Cz} = 0,\ T = T_m$$

in zone F:

$$v_{Cx} = 0,\ v_{Cz} = 0,\ T = T_s$$

(Note that $y = 0$ is the melt/solid bed interface in zone C and the screw flight in zone F, respectively.)

In this iterative procedure, it is necessary to make use of a boundary condition at $y = 0$ in the energy equation (11) which effectively defines the melting rate. Thus the melting rates in equation (3) are calculated only after the iterations for temperature and velocity profiles, for $\delta_C(z)$ and ψ_1, ψ_2 have converged. We have:

$$v_{Ay} = \frac{k_m \left.\frac{dT}{dy}\right|_{y=0}}{\{\lambda + C_s(T_m - T_s) + FC_m(\bar{T} - T_m)\}\rho_s} \tag{15}$$

where $\bar{T}$ is an average temperature calculated from an equation similar to equation (9).

Equation (15) is derived from equation 18a of Part I (for details see Pearson, 1976[4]). For the value of the parameter F, which depends upon generation, see below. Finally, using a continuity equation:

$$\rho_s v_{Ay} = \rho_m \frac{\partial m_{Cz}}{\partial z}$$

with

$$\frac{\partial m_{Cz}}{\partial z} = \frac{d}{dz}\int_0^{\delta_C(z)} v_{Cz}(y)dy$$

we obtain from equation (13) an equation for the size of zone C, $\delta_C(z)$:

$$\delta_C(z) = \delta_C(z=0) + \int_0^{z}\frac{\rho_s v_{Ay}}{\rho_m \int_0^{\delta_C(u)} v_{Cz}(y)dy}\,du \tag{16}$$

Using equations (13) and (14) we obtain R_C in equation (5) (this is equation 36 from Part I), and from:

$$S_{ACx} = \int_{\delta_E}^{\delta_E + Z}\left.\mu\frac{\partial v_{Cx}}{\partial y}\right|_{y=0} dz \tag{17}$$

whereby $\partial v_{Cx}/\partial y$ is taken at the melt/solid bed interface, we obtain S_{ACx} as required for equation (2).

We turn now to the analysis of zones D and E, i.e. the thin layers of molten polymer between solid bed and screw root and solid bed and screw flight. The analysis is carried out only when the screw is not cooled below melting temperature. The calculations are rather similar to those of zone C. It is assumed that all material melted at the AD and AE interfaces is trapped in zones D and E, respectively. Thus we have no flow in the z-direction in zone D nor in zone E.

The stress equilibrium equations become simply:

$$\frac{\partial}{\partial y}\left(\mu\frac{\partial v_{Dx}}{\partial y}\right) = \frac{\partial p}{\partial x}$$

with $v_{Dx}(0) = 0$ and $v_{Dx}(\delta_D) = v_{Ax}$.

Again μ is given by equation (7) but I_2 reduces to

$$I_2 = \frac{1}{4}\left(\frac{\partial v_{Dx}}{\partial y}\right)^2$$

(see equation 8).

```
POLYMER SCIENCE AND ENGINEERING GROUP
DEPARTMENT OF CHEMICAL ENGINEERING AND CHEMICAL TECHNOLOGY
UNIVERSITY OF LONDON, IMPERIAL COLLEGE
MELTING ZONE PROBLEM IN EXTRUSION PRESSURE DIFFERENCE SPECIFIED.
**********************************************************


PROBLEM SPECIFICATION
*********************


SCREW DIMENSIONS
****************
SCREW HELIX ANGLE                                17.66 DEGREES
BARREL DIAMETER                                  63.5000 MM.
AXIAL LENGTH IN MELT FILLED ZONE                 57.1500 MM.
CHANNEL SECTION WIDTH                            54.4577 MM.
CHANNEL DEPTH IN FEED ZONE                        9.9100 MM.
CHANNEL DEPTH IN METERING ZONE                    3.3000 MM.
HELICAL LENGTH OF COMPRESSION ZONE                1.0468  M.
FLIGHT GAP OR CLEARANCE                           .1000 MM.
FLIGHT WIDTH                                     6.3500 MM.

PROPERTIES OF THE MELT
**********************
POWER-LAW INDEX S                                 .2885
                n                                 .4230
POWER-LAW CONSTANT C(n)                       6274.0000 N.(SEC.)1-25/(M.)2
VISCOSITY SCALE FOR NON-DIMENSIONALIZING        78.2508 N.SEC./(M.)2 BASED ON THE FLIGHT GAP
REFERENCE TEMPERATURE T(n)                     145.0000 DEGREES C.
TEMPERATURE SENSITIVITY B                         .0054 (C. DEGREES)-1
THERMAL CONDUCTIVITY                              .2680 W./M.C.
DENSITY                                        780.0000 KG/(M.)3
HEAT CAPACITY OF THE MELT                     2428.0000 J./KG.CDEG.

PROPERTIES OF THE SOLID
***********************
THERMAL CONDUCTIVITY                              .2680 W./M.C.
DENSITY                                        880.0000 KG/(M.)3
HEAT CAPACITY OF THE MELT                     2512.0000 J./KG.CDEG.
MELTING TEMPERATURE                            110.0000 DEGREES CELSIUS
LATENT HEAT OF FUSION                          209350.0 J./KG

OPERATING CONDITIONS
********************
FLOWRATE                                          .1602E-04 (M.)3/SEC.
                                                  .0141 KG./SEC.
BARREL TEMPERATURE                             220.0000 DEGREES C.
SCREW  TEMPERATURE                             120.0000 DEGREES C.
FEED  TEMPERATURE                               30.0000 DEGREES C.
TEMPERATURE SCALE FOR NON-DIMENSIONALIZING      11.6199 DEGREES C. BASED ON THE FLIGHTGAP
CHANNEL PRESSURE GRADIENT                       32.9691 MN./(M.)3
AXIAL PRESSURE GRADIENT                          1.0000 MN./(M.)3
PRESSURE SCALE FOR NON-DIMENSIONALIZING          1561.0 SEC./(M.)2  BASED ON THE FLIGHTGAP
DIMENSIONLESS PRESSURE GRADIENT                   .0211
SCREW SPEED                                      1.0000 REV./SEC.
RELATIVE LINEAR VELOCITY                          .1995 M./SEC.
DOWN-CHANNEL VELOCITY COMPONENT                   .1901 M./SEC.
TRANSVERSE VELOCITY COMPONENT                     .0605 M./SEC.
THE INCREMENT USED IN THE ANALYSIS OF ZONE C     2.7229 MM.
THE INCREMENT USED IN DOWN-CHANNEL DIRECTION      .1047 M.
I.E. EACH STEP IN THE ANALYSIS CORRESPONDS TO     .5000 TURN

THE DIMENSIONLESS NUMBERS --- BASED ON THE FLIGHTGAP
***************************************************
PECLET NUMBER                          140.9717
GRIFFITHS NUMBER                         .3627
REYNOLDS NUMBER                          .00019885
GRAETZ NUMBER                           2.2200
```

The energy balance equation is exactly the same as in zone *C*, with boundary conditions becoming:

$$T(0) = T_s \text{ and } T(\delta_D) = T_m$$

The flow rate is given by:

$$m_{Dx} = \rho_{m0} \int_0^{\delta_D} v_{Dx} dz$$

Thus the melting rate in zone *D* is equal to:

Table 2 Solution control parameters

(a) Initial guesses

dp/dx = 1		MN/m^3 *
$\delta_D(1)$ = 0.4		mm*
$\delta_E(1)$ = 0.4		mm*
ψ_1 = 1		†
ψ_2 = −0.5		†

(b) Constraints

(i) Tolerance limits

$\psi_1-\psi_2$ iteration	0.001
Temperature profile iteration	0.001
δ_C, δ_D, δ_E iteration	0.001
dp/dx iteration	0.01

(ii) Maximum allowed limit

Size of zone *D, E*	3 mm
Flow rate of zone *A*	95% of M_T
Width of zone *A*	10% of *W*
Height of zone *A*	20% of *H*
Velocity of zone *A*	300% of initial v_{Ax}
Acceleration of zone *A*	50%

(c) Maximum number of points calculated

In *x*-direction	21
y-direction	21
z-direction	21

* See Appendix
† See above for definition

$$R_D = \frac{\partial m_{Dx}}{\partial x} Z \tag{18}$$

and the shear stress:

$$S_{ADx} = \left(\mu \frac{\partial v_{Dx}}{\partial y}\right) Z \tag{19}$$

Using exactly the same analysis for zone E, we obtain:

$$R_E = \frac{\partial m_{Ex}}{\partial x} (H - \hat{\delta} - \delta_D) \tag{20}$$

$$S_{AEx} = \left(\mu \frac{\partial v_{Ex}}{\partial y}\right) (H - \hat{\delta} - \delta_D) \tag{21}$$

with boundary conditions for the temperature and velocity fields given by

$$T(y) = T_m,\ v_{Ex}(y) = v_{Ax} \quad \text{for } y = 0$$

$$T(y) = T_s,\ v_{Ex}(y) = 0 \qquad \text{for } y = \delta_E$$

(see Part I and *Figure 1b* for the varying use of y).

We note that in the early stages of the melting process, the width of zone B is comparable with that of zones D and E. In such cases we apply an analysis similar to that of zones D and E rather than equation (6), i.e. the Rowell–Finlayson model, keeping in mind that the size of zone B is given by:

$$\bar{W} = W - Z - \delta_E$$

and thus need not be calculated.

TYPICAL NON-NEWTONIAN SOLUTION

Table 1 gives: (a) geometrical data in a typical 2½ in single screw extruder; (b) physical data for a low density polyethylene (LDPE); (c) 'typical' operating conditions (it has been noted that the barrel temperature may seem some 30°–40°C higher than usual, but this is highly dependent on the polymer process being carried out). In what follows, we shall refer to the numerical solution with input data given in *Tables 1* and *2* as the 'Standard' solution to distinguish it from other solutions with altered operating conditions.

We describe first the sequence of steps that take place when the computer program is run for a typical case before describing the numerical results obtained when certain operating conditions were varied. The analysis covers the compression zone (of a single screw extruder) and assumes that at the start, thin layers of molten material have already formed in zones *B, C, D,* and *E*†. The size of these layers is chosen to be part of the input data. When the analysis starts at the beginning of the compression zone, it advances in prescribed steps in the x-direction (with a step size of 1, 1/2, 1/5, etc. turns). After the analysis has been completed at any one stage (each step leads to a new stage in the calculations) the current values of the main variables are printed out. The analysis is stopped when one of the following conditions occurs, in which case the final results of the analysis are printed out (see *Table 3* for a list of these):

(a) the processor's time limit is nearly reached;

(b) the maximum number of stages (i.e. 21) for any one run is reached;

(c) one of the various criteria which imply that the solid bed might have broken up is satisfied (see Appendix 1 for a list).

If one of the first two events stops the analysis the processor can be restarted using the last completed set of results as input data for a new run. This can be repeated any number of times. When the analysis stops because a criterion belonging to the last group is satisfied, the processor cannot be restarted. These criteria are connected with the assumptions made when the 6 zone model was formulated; when

† By using zero compression, the melting in a constant depth channel can be simulated, and can then be used as the input information to a succeeding compression section.

Table 3 Variables given in final print out

1	Coordinates in *x, y* and *z*-direction
2	Screw temperature (as a function of *x*)
3	Size of zones *D* and *E* (as a function of *x*)
4	Melting rates per unit width in zones *C, D,* and *E*
5	Shear forces per unit length in *x*-direction in zones *C, D,* and *E* (as a function of *x*)
6	Flow rate per unit length in *x*-direction in zones *D* and *E* (as a function of *x*)
7	Width of zone *A* (as a function of *x*)
8	Mean height of solid bed (as a function of *x*)
9	Molten polymer swept into pool from zone *C* (as a function of *x*)
10	Pressure gradient (as a function of *x*)
11	Pressure within extruder (as a function of *x*)
12	Axial velocity of solid bed (as a function of *x*)

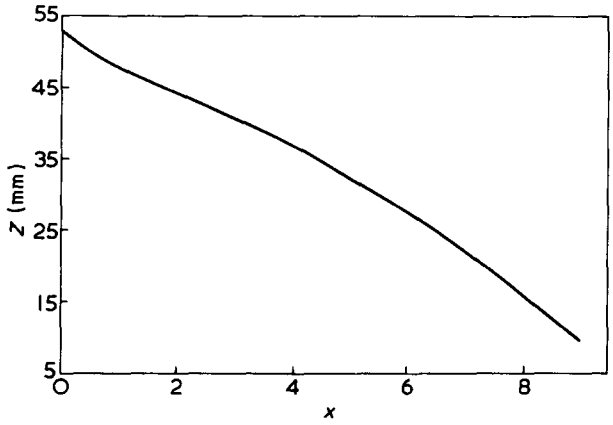

Figure 2 Z vs. x

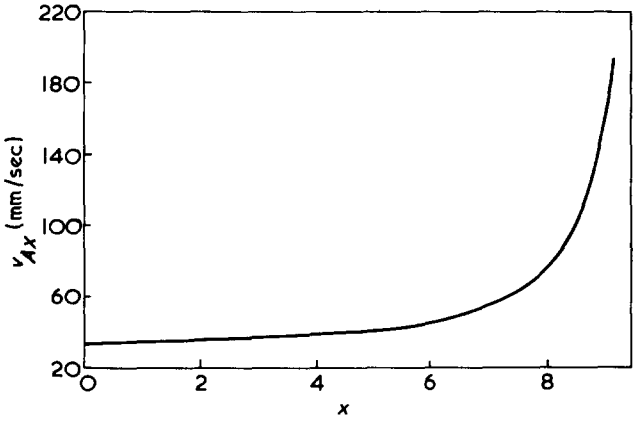

Figure 3 v_{Ax} vs. x

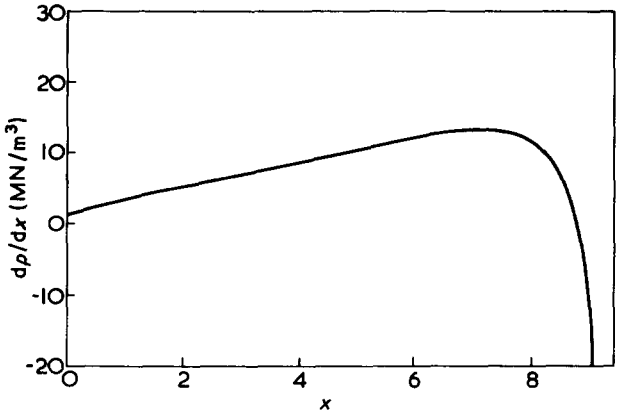

Figure 4 dp/dx vs. x

violated the iterative scheme would produce an unacceptable solution and possibly not converge at all.

We shall not describe the predictions for the 'standard' solution as produced by the computer. The abscissa x is measured in turns with turn no. 0 being the beginning of the compression zone and turn no. 10 the beginning of the metering zone of a single screw extruder. For the screw geometry given here (see *Table 1*) one turn corresponds to 0.2094 m helical distance in the x-direction. (Thus five turns are approximately 1 m.)

In *Figures 2–9* predictions are given for Z, v_{Ax}, dp/dx, δ_D, R_C, R_D, R_E, S_{ACx}, S_{ADx}, S_{AEx}, μ and $\bar{T}$. The graphs show essentially the same trends of pressure and velocity development as obtained earlier (Part II). However, since a constant viscosity was assumed in Part II it is difficult to compare in detail the actual values of the melting parameter.

To indicate this difficulty, *Figures 10–13* are of interest. Here dp/dx, v_{Ax}, Z and μ are plotted when the power law index s varies over a range from 0.0 to 0.45. The different values for s and the corresponding values for the consistency index C_0 are given below. (C_0 is measured at reference temperature T_0 and constant shear rate using a mean velocity gradient of 30 sec^{-1}.)

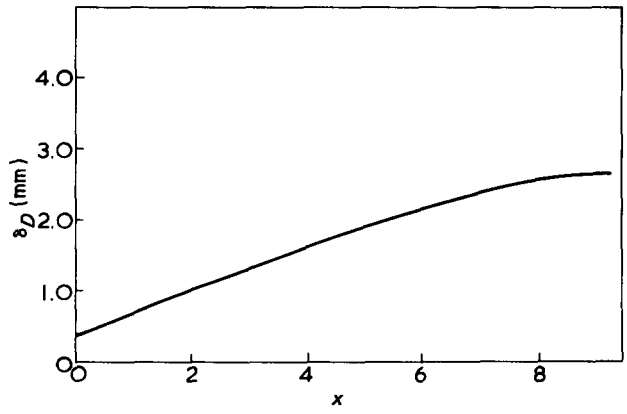

Figure 5 δ_D vs. x

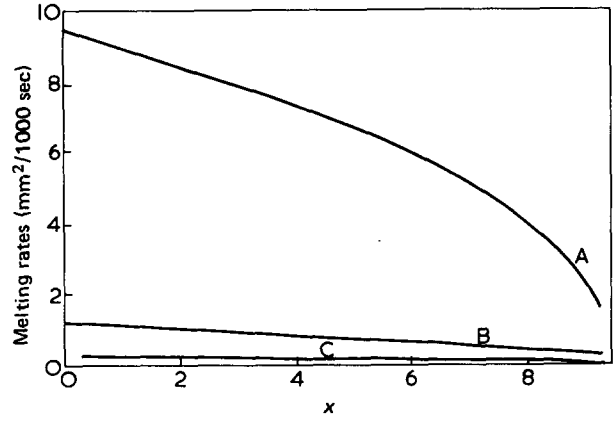

Figure 6 R_C, R_D, R_E vs. x; A, Zone C; B, Zone D; C, Zone E

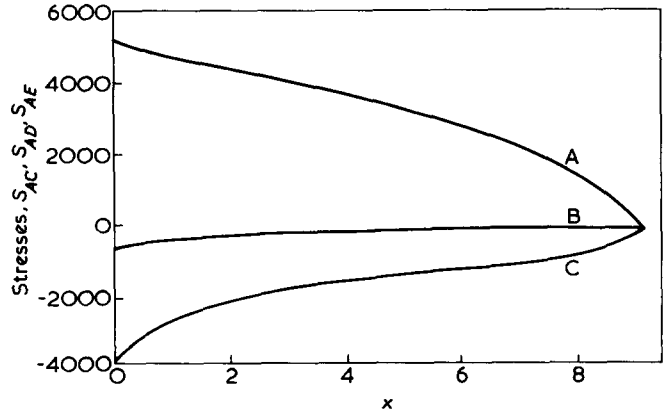

Figure 7 S_{ACx}, S_{ADx}, S_{AEx} vs. x: A, Zone C; B, Zone E; C, Zone D

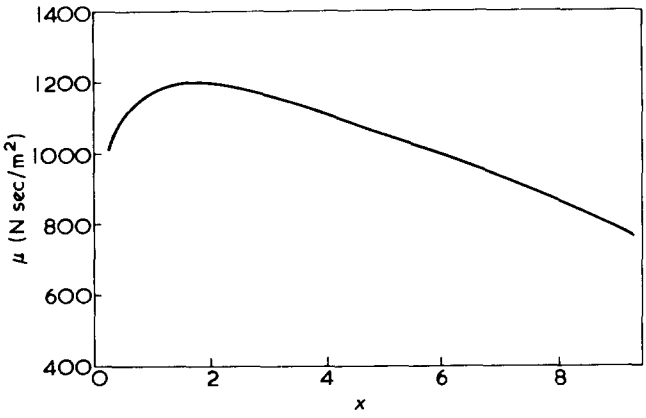

Figure 8 μ vs. x. (See equation 7)

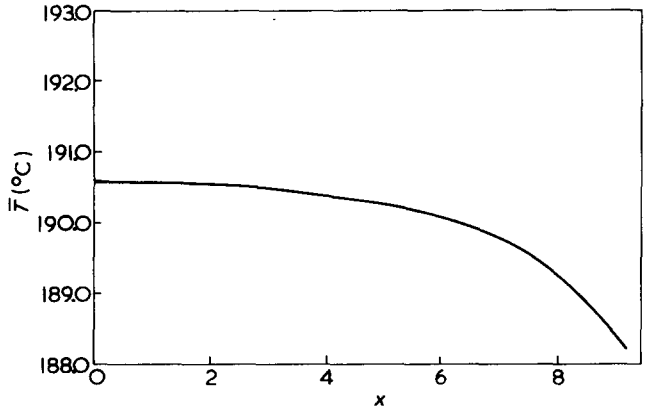

Figure 9 $\bar{T}$ vs. x. (See equation 9)

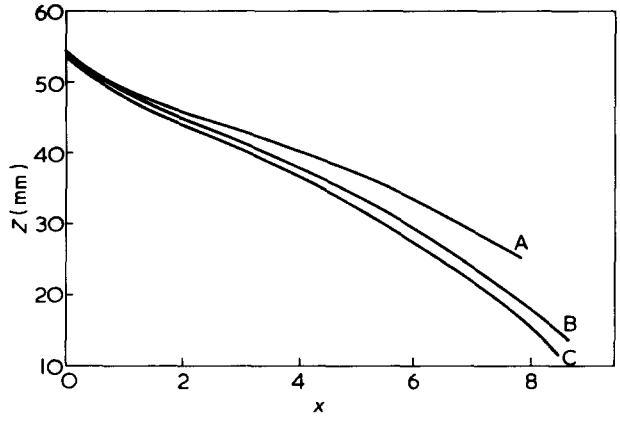

Figure 10 Z vs. x. A, s = 0.45; B, s = 0.35; C, s = 0.2885

Run number	s	C (N sec^{1-2s}/m^2)
1	0.0	123.8
2	0.1	482.8
3	0.2	1883.5
4	0.2885	6274.0
5	0.35	14484.0
6	0.45	56464.0

Before proceeding with some variations of the operating conditions, a remark about certain features of the numerical scheme is called for. One can distinguish between three essentially different phases of the predicted melting process which might or might not reflect upon real events. The first phase is described by a slightly faster decrease in Z (*Figure 2*) during the first few stages (see also *Figures 6* and *7*) than occurs once the solution has 'settled down'. The middle phase is characterized by smooth and nearly linear behaviour of Z and dp/dx (*Figures 2* and *3*). This might indicate that the program calculates almost a similarity solution for these main melting parameters. Finally, we have a phase during which the solid bed accelerates rapidly and the pressure

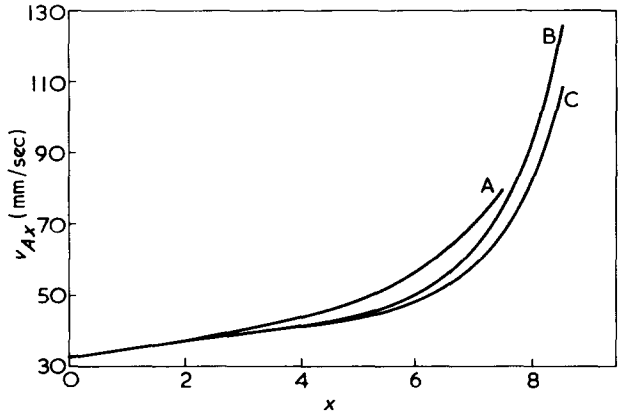

Figure 11 v_{Ax} vs. x. s values: A, s = 0.45; B, s = 0.2; C, s = 0.2885

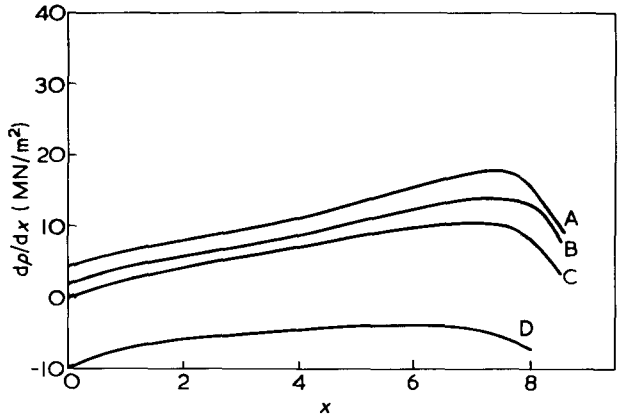

Figure 12 dp/dx vs. x. A, S = 0.2; B, S = 0.2885; C, S = 0.35; D, S = 0.45

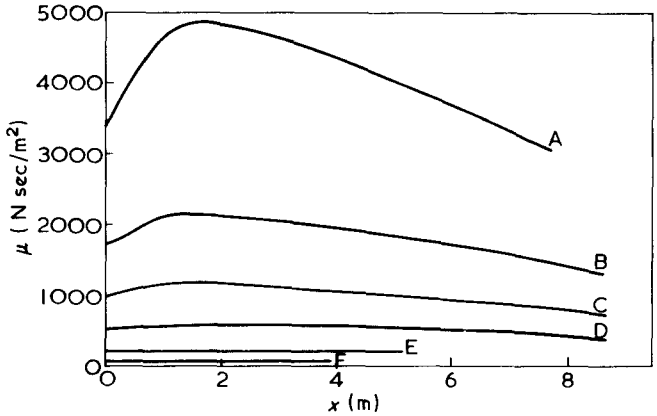

Figure 13 μ vs. x. s values; A, 0.0; B, 0.1; C, 0.2; D, 0.2885; E, 0.35; F, 0.45

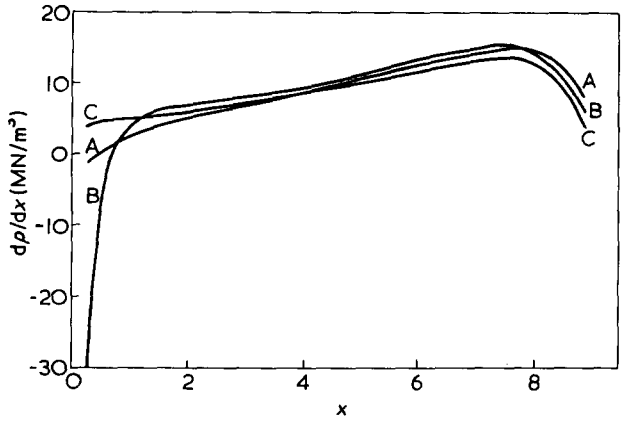

Figure 14 dp/dx vs. x. δ_D values: A, 0.2 mm; B, 0.1 mm; C, 1.0 mm

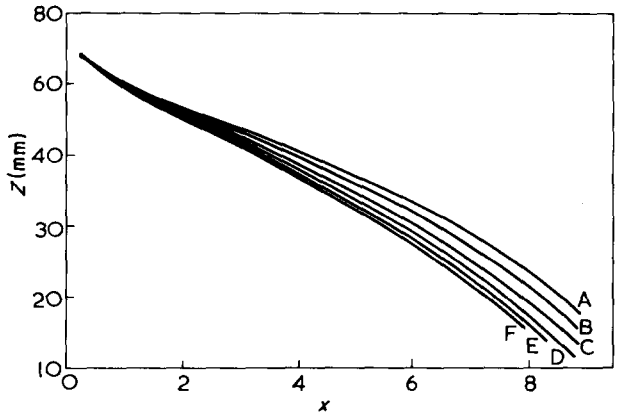

Figure 15 Z vs. x. T_b values (°C): A, 160; B, 180; C, 200; D, 220; E, 240; F, 260

gradient dp/dx reaches a maximum and decreases (around turn no. 7 or 8). It seems plausible that this last effect is due to the fact that the depths of the zones D and E which were assumed to be small compared with H become of the same order as H. The starting effect can be eliminated or altered by varying the initial value of δ_D (and δ_E) (see *Figure 14*). From this point of view δ_D = 0.44 mm seems the most realistic initial value for the given set of screw and polymer input data.

Finally, it should be noted that divergence from smoothness between turns 2 and 4 (see *Figures 3* and *4* and S_{ACx}, S_{AEx} in *Figure 7*) is due to the tolerance limits chosen for numerical purposes, and is probably not a real effect.

The results of making certain variations in the operating conditions on the standard solution are now described. Although some of these are somewhat artificial, they indicate how the results of numerical calculations depend upon the variables.

We start by varying the barrel temperature from 160° to 260°C. *Figure 15* shows the effect on the melting length which is slightly shortened with increase in barrel temperature. [By slightly it is meant that the point when 50% of the polymer has melted lies within one turn. This represents a 15–20% change in melting length for a 3-fold change in $(T_b - T_m)$.] An increase in the barrel temperature increases the melting rate at the solid bed/barrel interface, thus increasing the size of zone C. On the other hand, it causes the viscosity (given in equation 7) to decrease (see *Figure 16*), hence the stress in zone C decreases (see equation 17). Consequently, dp/dx decreases with increasing barrel temperature, as shown in *Figure 17*. v_{Ax} is relatively unaffected by a change in barrel temperature (see *Figure 18*).

Next we vary the screw temperature. We have plotted two entirely different screw temperature profiles. First, T_s is varied linearly from 120°, 140° or 160°C at the start of the compression zone to 220°C at the end of it. Then the screw temperature was kept constant at 120°, 150° and 180°C. Both approaches are really approximations to the

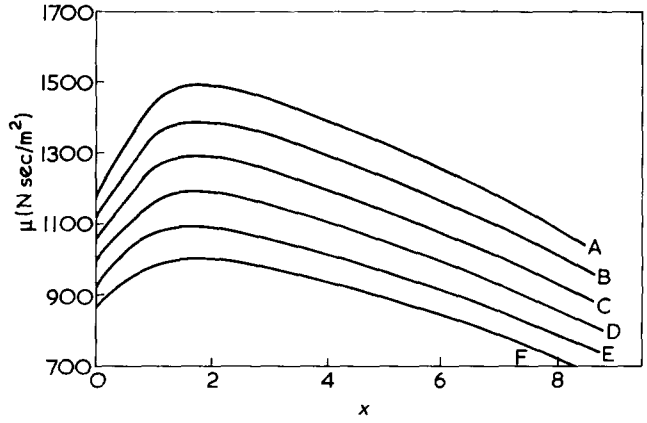

Figure 16 μ vs. x. T_b values (°C): A, 160; B, 180; C, 200; D, 220; E, 240; F, 260

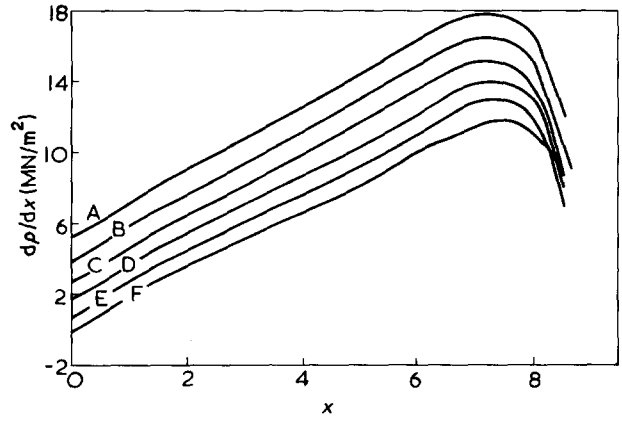

Figure 17 dp/dx vs. x. T_b (°C); A, 160; B, 180; C, 200; D, 220; E, 240; F, 260

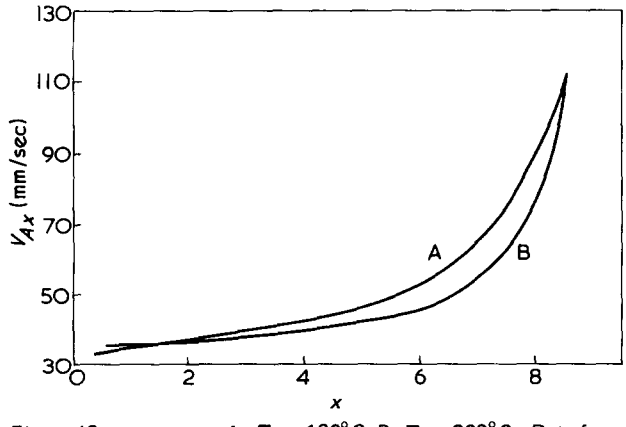

Figure 18 v_{Ax} vs. x. A, T_b = 160°C; B, T_b = 260°C. Data for T_b between 160° and 260°C fall in between

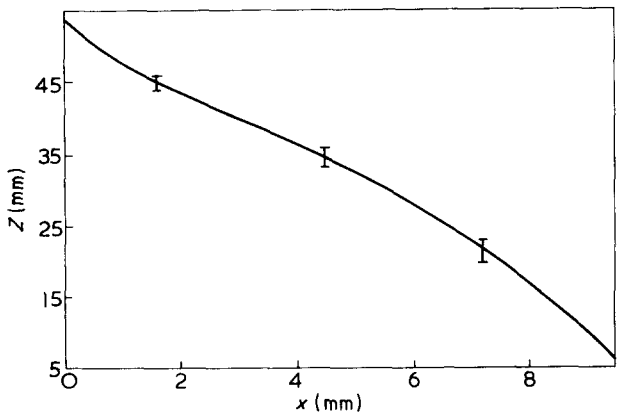

Figure 19 Z vs. x. Range of T_S, 120°–180°C covered by error bars

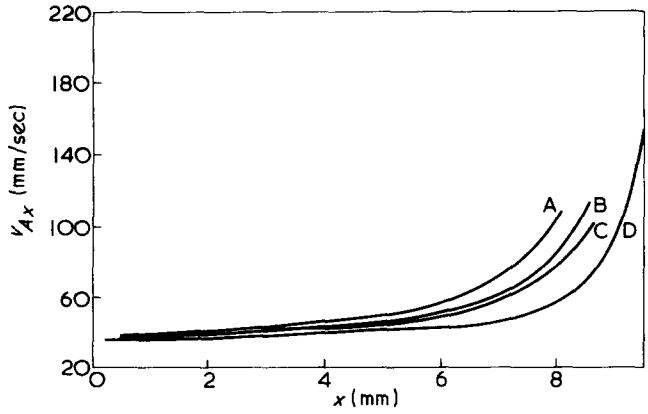

Figure 20 v_{Ax} vs. x. A, T_S = 160°C (variable); B, 120°C (variable); C, 150°C (constant); D, 120°C (constant)

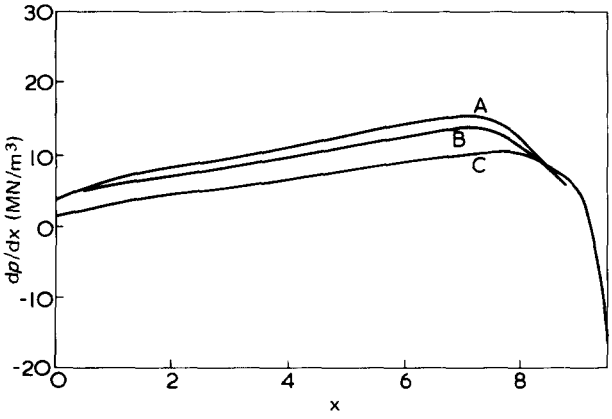

Figure 21 dp/dx vs. x. A, T_S = 160°C; B, T_S = 180°C (constant); C, T_S = 120°C (constant)

true situation, when the screw is heated by conduction and convection through the melt layers between screw root or flight and barrel. *Figure 19* shows that there is virtually no effect on the predicted melting length. The effect on v_{Ax} (*Figure 20*) and dp/dx (*Figure 21*) is slightly larger but not very significant, disregarding the case when T_S is kept constant at 120°C. That a screw temperature of constant 120°C is extremely low compared with the other cases can be seen best in *Figure 22*. Here, as one would expect, the size of zone D increases less with lower T_S. This suggests *a posteriori* that a linearly varying screw temperature profile such as we have chosen will not lead to gross errors.

We now vary the mass flow rate M_T (keeping all the other parameters constant). This is a very severe requirement and is unlikely to be achieved in practice. Nevertheless, certain trends are shown which will be of interest later on. The most clear (and necessary) effect of increased mass flow rate is that v_{Ax} increases (*Figures 23*) while dp/dx decreases (*Figure 24*). In reality it is often a change in the latter due to a change of die geometry that will cause M_T to change.

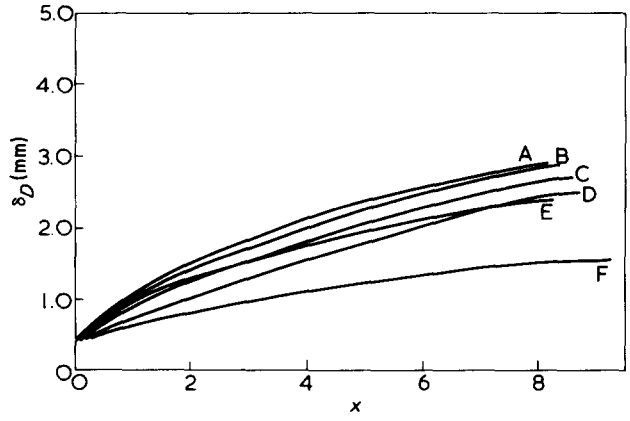

Figure 22 δ_D vs. x. A, T_S = 180°C (constant); B, T_S = 160°C (variable); C, T_S = 140°C (variable); D, T_S = 120°C (variable); E, T_S = 150°C (constant)

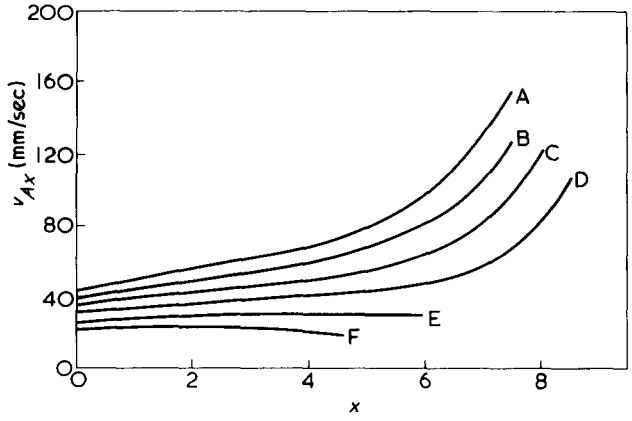

Figure 23 v_{Ax} vs. x. M_t values: A, 20; B, 18; C, 16; D, 14; E, 12; F, 10 (g/sec)

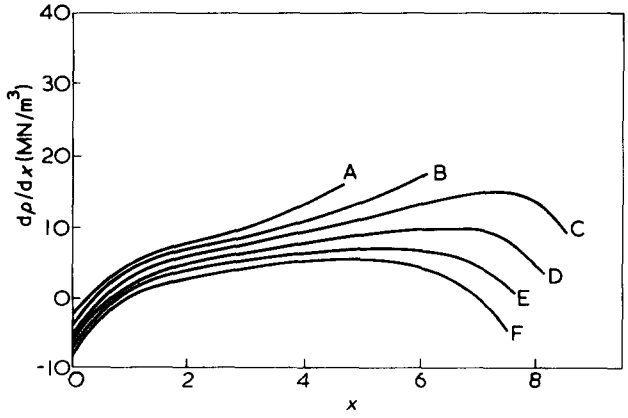

Figure 24 dp/dx vs. x. M_t values: A, 10; B, 12; C, 14; D, 16; E, 18; F, 20 (g/sec)

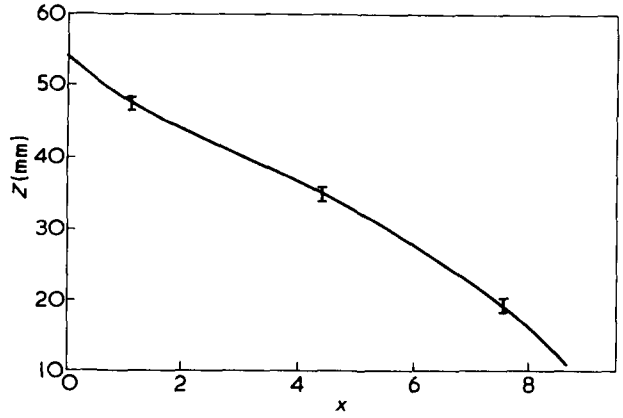

Figure 25 Z vs. x. Range of M_t: 10–20 covered by error bars

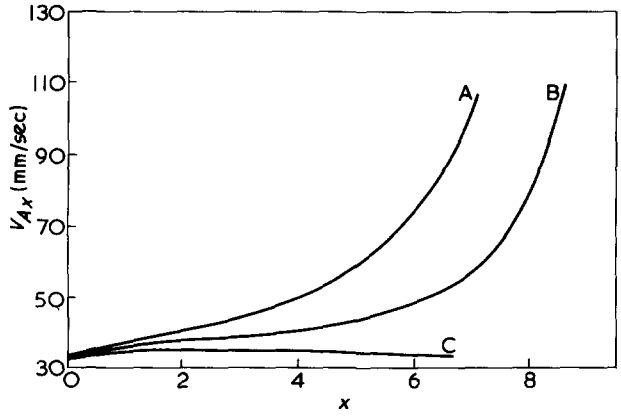

Figure 26 v_{Ax} vs. x. A, 40 rpm; B, 60 rpm; C, 80 rpm

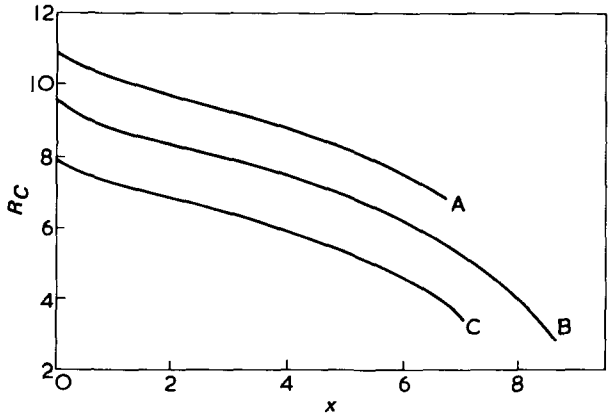

Figure 27 R_C vs. x. A, 80 rpm; B, 60 rpm; C, 40 rpm

The length of the melting zone (*Figure 25*) is almost unchanged, a striking testimony to the flexibility of the plasticating extruder.

We now consider variations of the rate of revolution N. *Figure 26* shows a very large change in v_{Ax} as the solid bed melts. The total melting increases with increased N (*Figure 27*), despite the apparent increase in width (*Figure 28*) at any given x because v_{Ax} has risen much less. *Figure 29* shows the effect on dp/dx.

Finally we vary M_T and N simultaneously, keeping the dimensionless flow rate:

$$M_T^* = M_T/WHv_{bx}$$

constant. This simulates real situations rather better than varying one parameter only. *Figure 30* shows the varying melting length which, compared with *Figure 25* or *Figure 28*, shows significant deviations from the standard solution. The changes in v_{Ax} (*Figure 31*) are not very different from those obtained when varying M_T alone (*Figure 23*). The simultaneous change in M_T and N seems to be compensating when

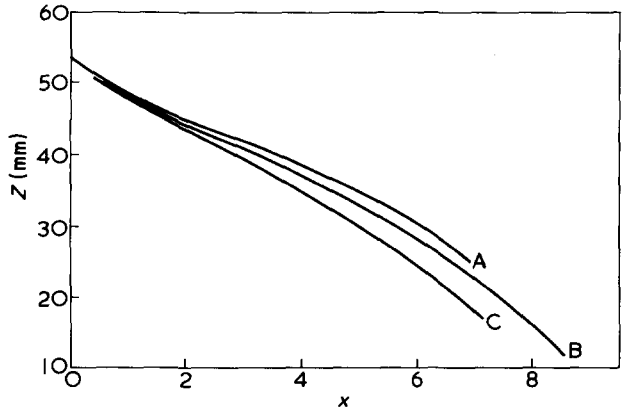

Figure 28 Z vs. x. A, 80 rpm; B, 60 rpm; C, 40 rpm

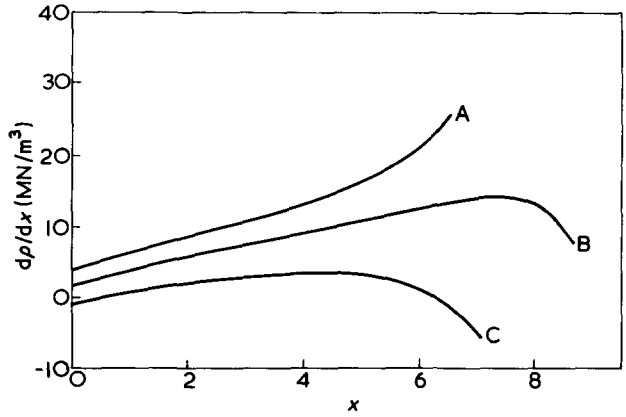

Figure 29 dp/dx vs. x. A, 80 rpm; B, 60 rpm; C, 40 rpm

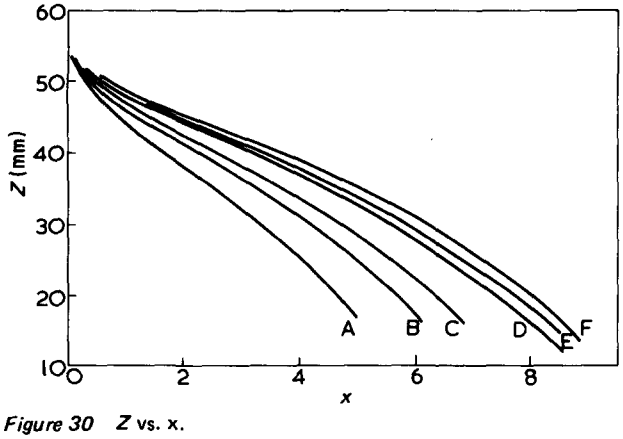

Figure 30 Z vs. x.

Curve	M_t (g/sec)	N(rpm)
A	4.7	20
B	7.0	30
C	9.4	40
D	14.1	60
E	16.5	70
F	18.8	80

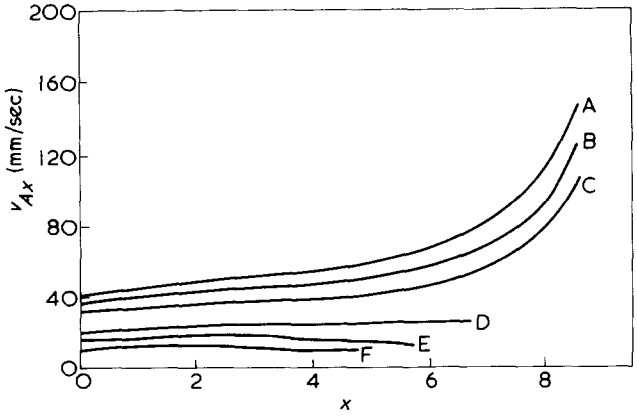

Figure 31 v_{Ax} vs. x.

Curve	M_t (g/sec)	N (rpm)
A	18.8	80
B	16.5	70
C	14.1	60
D	9.4	40
E	7.0	30
F	4.7	20

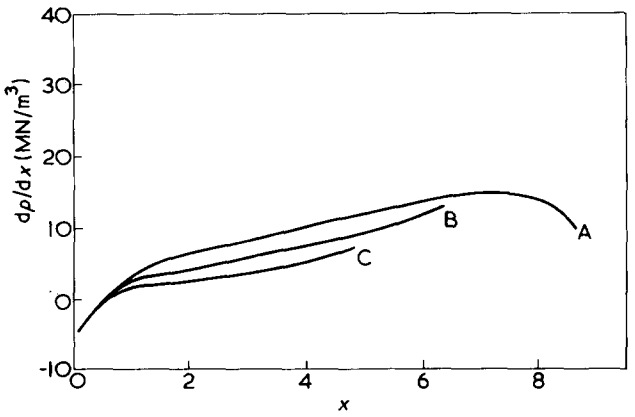

Figure 32 dp/dx vs. x

Curve	M_t (g/sec)	N (rpm)
A	18.8	80
B	9.4	40
C	4.7	20

considering dp/dx (*Figure 32*). Perhaps most interesting is that when varying M_T alone there is virtually no effect on the melting rate per unit distance in the x-direction (*Figure 33*). But when changing both M_T and N simultaneously, M_{Cx} increases considerably (*Figure 34*).

In conclusion, it is necessary to make a few remarks about certain assumptions which we made implicitly. First, it was assumed that the bulk of the solid bed remains at the feed temperature. Varying the feed temperature over a range from 30° to 80°C has little effect on the predicted solutions. The melting length is slightly shorter with increased feed temperature as one would expect.

A priori it is doubtful whether the flight clearance can be kept at a constant value (we take $\delta_F = 0.1$ mm throughout). In practice, the screw will wear out in places and perhaps vibrate slightly during production runs. Extensive tests have been carried out to determine the influence of a variable flight gap on predicted melting length and pressure generated. The melting length turns out to be slightly longer for a flight gap of 0.15 mm and correspondingly shorter for a flight gap of 0.05 mm. Similarly, the predicted pressure gradient is slightly larger for the smaller flight gap and correspondingly smaller for the larger flight gap. The effect on v_{Ax} is negligible. Thus the program shows expected sensitivity to changes in the flight gap δ_F, although these are not dominant. On the other hand, one can change the flight gap randomly from stage to stage between maxima and minima of 0.15 and 0.05, respectively. The deviation from the standard flight gap of 0.1 mm is less than 0.5% for the predicted value of Z, less than 1.5% for v_{Ax} and less than 5% for the predicted value of dp/dx, when the flight gap varies randomly.

Finally, we note the initial film thickness in zones B, D and E. The value of $\delta_D(1)$ and $\delta_E(1)$ reflects the melting process before the analysis of this program starts and thus has to be given as input data which will (even if only slightly) affect the overall results. Nevertheless, for the input data of the standard solution (*Tables 1* and *2*) the predicted melting length, the predicted pressure gradient (*Figure 14*), and the predicted axial velocity of the solid

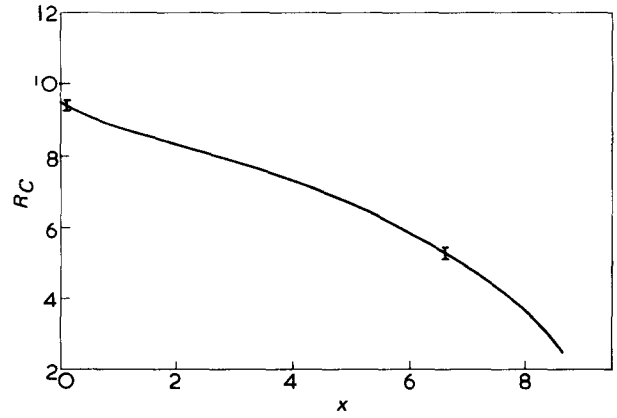

Figure 33 R_C vs. x. M_t: 10–20 (g/sec)

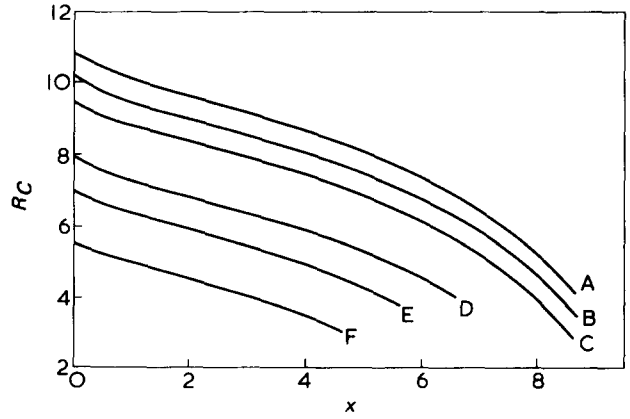

Figure 34 R_C vs. x

Curve	M_t (g/sec)	N (rpm)
A	18.8	80
B	16.5	70
C	14.1	60
D	9.4	40
E	7.0	30
F	4.7	20

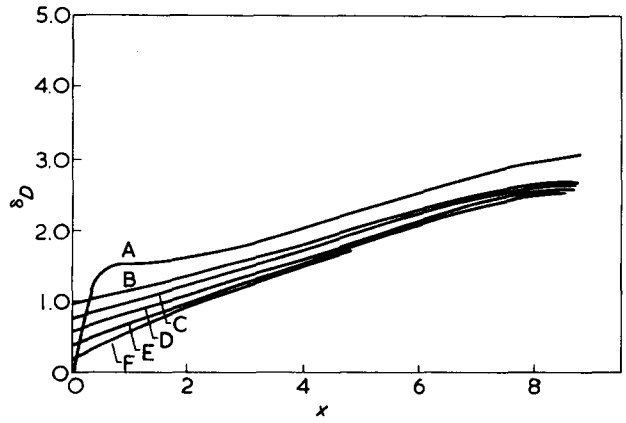

Figure 35 δ_D vs. x: $\delta_D(1)$ values; A, 0.01; B, 1.0; C, 0.8; D, 0.6; E, 0.4; F, 0.2

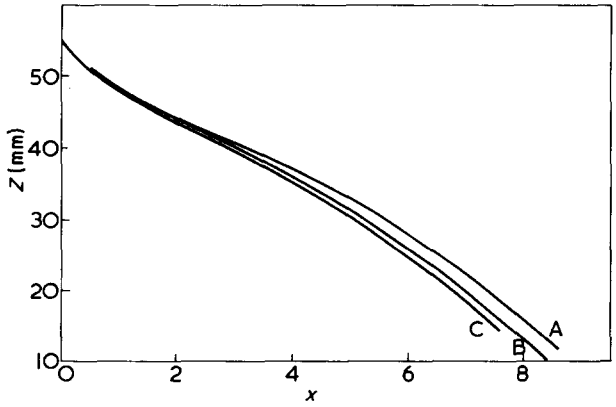

Figure 36 Z vs. x. A, F = 1.0; B, 0.5; C, 0.25

bed are very little altered when $\delta_D(1) = \delta_E(1)$ varies in the range of 0.2 to 0.8 mm. The effect on the size of zone D and E is given in *Figure 35*. (An initial layer thickness of 0.01 mm appears to be extremely low for the given set of input data.) Changes in $\bar{W}$ are even less important.

VERIFICATION OF ASSUMPTIONS

Using the numerical results given above we are now able to verify *a posteriori* the validity of the original assumptions made when formulating the 5 zone model in Part I of this paper.

δ_C

The size of zone C is given as a function of x and z in *Table 4*. *Table 5a* gives the varying values of $(\delta_C/H)_{max}$ with a maximum of 0.07. It can be seen from *Table 4* that $\partial\delta_C/\partial z$ has its maximum 0.02 near the flight. *Table 5b* gives the maxima of $\partial\delta_C/\partial x$ as a function of x. At 0.0003 it is very small, as expected. These are fully consistent with the original assumption on the slowly changing nature of δ_C.

δ_D *and* δ_E

Figure 5 shows the varying size of zones D and E and *Table 5c* gives the values for δ_D/H with a maximum of 0.66 at the end of the compression zone. Thus δ_D/H cannot be neglected and the use of $\bar{H}$ instead of H in the overall equations is essential. The growth of δ_D in absolute terms is however not so marked, but the assumptions inherent in the original 6 zone model (in particular, absence of z-flow in zone D and y-flow in zone E) cannot be said to hold after turn 5. This corresponds to the point at which almost 65% of the granule feed was melted. Predictions for later stages have to be treated with some caution.

v_{Ax} *and* Z

The lubrication approximation for zones C, D and E assumed that v_{Ax} and Z are slowly varying with x, i.e.:

$$\frac{\delta_I}{v_{Ax}}\frac{\partial v_{Ax}}{\partial x} \ll 1$$

Tables 5d and *5e* shows the values for $I = C$ and $I = D$ respectively. Since the maximum is smaller than 0.0005 for zone C and smaller than 0.0006 for zones D and E, the lubrication approximation is entirely justified.

In *Tables 5f* and *5g* the values for:

$$\frac{W}{v_{Ax}}\frac{dv_{Ax}}{dx} \quad \text{and} \quad \frac{W}{Z}\frac{dZ}{dx}$$

are given with a maximum of 0.1. This justifies the assumption that Z and v_{Ax} are slowly varying functions of x when deriving equation (6a) in Part I, i.e. the stress balance equation.

R *and* S

The figures for

$$\frac{R_D + R_E}{R_C} \quad \text{and} \quad \left|\frac{S_{ADx} + S_{AEx}}{S_{ACx}}\right|$$

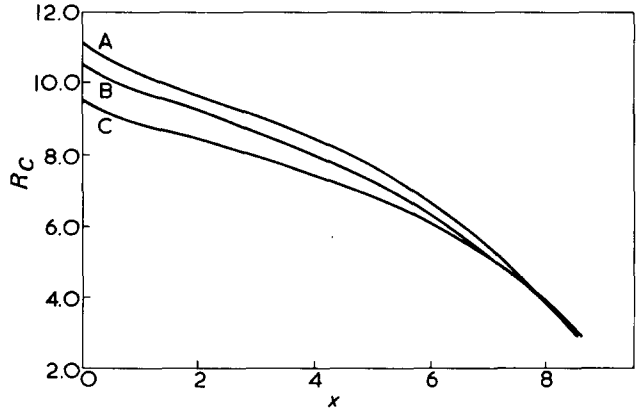

Figure 37 R_C vs. x. F values: A, 0.25; B, 0.5; C, 1.0

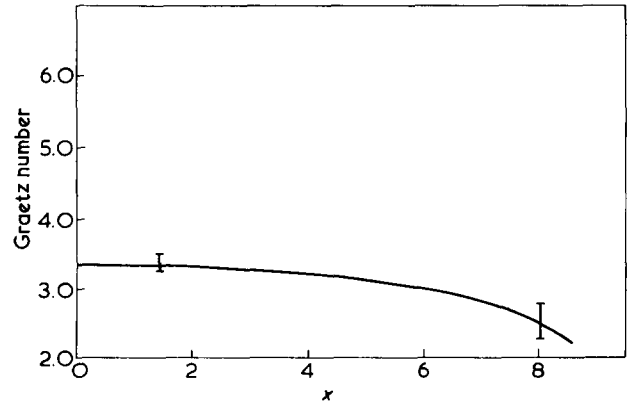

Figure 38 Graetz No. vs. x.

Table 4 Size of zone *C* in mm

	z									
x (mm)	0	2.7229	5.4458	8.1687	10.8915	13.6144	16.3373	19.0602	21.7831	24.5060
0	.0996	.1524	.1900	.2226	.2504	.2760	.2994	.3212	.3417	.3612
104.7	.0993	.1523	.1899	.2225	.2504	.2759	.2994	.3212	.3417	.3611
209.4	.0992	.1522	.1898	.2224	.2503	.2758	.2992	.3211	.3416	.3610
314.0	.0992	.1522	.1897	.2224	.2502	.2758	.2992	.3210	.3415	.3610
418.7	.0992	.1522	.1897	.2224	.2502	.2757	.2992	.3210	.3415	.3609
523.4	.0993	.1522	.1897	.2224	.2502	.2757	.2992	.3210	.3415	.3609
628.1	.0992	.1522	.1898	.2224	.2503	.2758	.2993	.3211	.3416	.3610
732.7	.0992	.1522	.1897	.2223	.2501	.2657	.2991	.3209	.3414	.3608
837.4	.0991	.1521	.1896	.2223	.2501	.2756	.2990	.3208	.3413	.3607
942.1	.0989	.1520	.1895	.2222	.2499	.2754	.2989	.3207	.3412	.3606
1046.8	.0986	.1519	.1893	.2220	.2498	.2753	.2987	.3205	.3410	.3604
1151.4	.0963	.1517	.1891	.2218	.2495	.2751	.2985	.3203	.3408	.3602
1256.1	.0973	.1515	.1889	.2216	.2493	.2748	.2982	.3200	.3404	.3598
1360.8	.0974	.1512	.1865	.2213	.2489	.2744	.2978	.3196	.3400	0
1465.5	.0975	.1511	.1884	.2210	.2486	.2740	.2973	.3190	0	0
1570.2	.0981	.1512	.1884	.2208	.2483	.2737	.2969	0	0	0
1674.8	.1005	.1519	.1890	.2210	.2484	.2735	0	0	0	0
1779.5	.1093	.1558	.1924	.2232	.2504	0	0	0	0	0

	z									
x (mm)	27.2288	29.9517	32.6746	35.3975	38.1204	40.8433	43.5662	46.2890	49.0119	51.7348
0	.3795	.3973	.4142	.4305	.4463	.4616	.4763	.4907	.5047	0
104.7	.3795	.3973	.4142	.4305	.4463	.4616	.4763	.4907	0	0
209.4	.3794	.3971	.4141	.4304	.4461	.4614	.4762	0	0	0
314.0	.3794	.3971	.4140	.4303	.4461	.4614	0	0	0	0
418.7	.3794	.3971	.4140	.4303	.4461	.4613	0	0	0	0
523.4	.3794	.3970	.4140	.4303	.4461	0	0	0	0	0
628.1	.3795	.3972	.4141	.4305	.4462	0	0	0	0	0
732.7	.3793	.3969	.4139	.4302	0	0	0	0	0	0
837.4	.3792	.3968	.4138	0	0	0	0	0	0	0
942.1	.3790	.3967	.4136	0	0	0	0	0	0	0
1046.8	.3788	.3965	0	0	0	0	0	0	0	0
1151.4	.3786	0	0	0	0	0	0	0	0	0
1256.1	0	0	0	0	0	0	0	0	0	0
1360.8	0	0	0	0	0	0	0	0	0	0
1465.5	0	0	0	0	0	0	0	0	0	0
1570.2	0	0	0	0	0	0	0	0	0	0
1674.8	0	0	0	0	0	0	0	0	0	0
1779.5	0	0	0	0	0	0	0	0	0	0

Table 5

		a		b	c	d	e	f	g	h	i	j
Turn No.	H	$\left(\frac{\delta_C}{H}\right)_{max}$	$\left(\frac{\partial \delta_C}{\partial z}\right)_{max}$	$\partial\delta_C/\partial x$	δ_C/H	$\frac{\delta_C}{v_{Ax}}\frac{\partial v_{Ax}}{\partial x}$	$\frac{\delta_D}{v_{Ax}}\frac{\partial v_{Ax}}{\partial x}$	$\frac{w}{v_{Ax}}\frac{\partial v_{Ax}}{\partial x}$	$\frac{W}{Z}\frac{\partial Z}{\partial x}$	$\frac{R_D+R_E}{R_C}$	$\frac{S_{AEx}+S_{ADx}}{S_{ACx}}$	$\frac{W}{P}\frac{dp}{dx}$
0	9.91	0.06	0.02	0.0003	0.01	1.8	1.5	0.04	0.04	0	1.4	0.029
1	9.25	0.06	0.02	0.0003	0.05	0.7	1.4	0.01	0.02	0.17	0.8	0.01
2	8.59	0.06	0.02	0.0003	0.1	1.5	1.5	0.011	0.034	0.15	0.6	0.02
3	7.93	0.06	0.02	0.0003	0.15	0.6	3.0	0.011	0.02	0.14	0.55	0.033
4	7.27	0.06	0.02	0.0003	0.2	0.9	3.0	0.016	0.03	0.13	0.52	0.037
5	6.6	0.06	0.02	0.0003	0.3	1.0	1.5	0.02	0.038	0.12	0.5	0.038
6	5.9	0.08	0.02	0.0003	0.35	1.7	30	0.04	0.05	0.11	0.54	0.04
7	5.3	0.08	0.02	0.0003	0.4	2.6	60	0.06	0.07	0.11	0.53	0.039
8	4.92	0.06	0.02	0.0003	0.55	3.8×10^{-4}	$\times 10^{-4}$	0.09	0.1	0.1	0.7	0.032
9	3.96	0.06	0.02	0.0003	0.66	3.8×10^{-4}	$\times 10^{-4}$					

With $P(0) = 10$ MN/m^2

are given in *Tables 5h* and *5i*. The latter shows that the stress balance must include the stresses at interfaces *AD* and *AE*. The former confirms that melting is dominated by the barrel–solid interactions.

The values for $(W/p)(dp/dx)$ as given by *Figure 5j* confirm that a locally isotropic state of pressure is dominant and so the freely deformable rheological model for the solid is not wholly without foundation.

Choice of thermal flux boundary condition

Following a suggestion made in Part II of this paper, calculations have been carried out for the parameter F in the energy balance equation (18), taking the values: $F = 0.25$, 0.5 and 1.0. In *Figures 42–44* we show its effect on Z, v_{Ax} and dp/dx which is significant but not dominant. *Figure 45* shows the effect of this variation on the melting rate in zone *C*.

Graetz number

Figure 40 shows the Graetz number used in the analysis of zone C for flow in the z-direction, which is $0(1)$ as assumed (see Pearson and Shapiro, 1974).

Finally we note that M^{-1} defined in Part I by:

$$M^{-1} = \frac{C_m(T_b - T_m)}{\lambda + (T_m - T_f)C_s}$$

has a value of 0.53, which is small as required to apply the energy balance equation (14).

ACKNOWLEDGEMENTS

The authors wish to thank the Science Research Council for financial support for this work.

REFERENCES

1 Rowell, H. S. and Finlayson, D. *Engineering* 1922, **114**, 606; 1928 **126**, 249, 385
2 Shapiro, J. *PhD Thesis* University of Cambridge (1973)
3 Shapiro, J., Halmos, A. L. and Pearson, J. R. A. *Polymer* 1976, **17**, 905, 918 (Parts 1 and 2 of the paper)
4 Pearson, J. R. A. *Int. J. Heat Mass Transfer* 1976, **19**, 405

NOMENCLATURE

A, B	constants as defined in equation (6)
b	a material constant in a constitutive equation (temperature sensitivity of apparent viscosity),
C_m, C_s	specific heat of melt, solid ($C_s = C_A$ from Parts I, II),
C_0	material constant in the constitutive equation,
D_b	barrel diameter,
F	constant introduced in equation (15),
f	a scalar function used in equation (6),
G	pressure gradient,
H	depth of screw channel,
$\bar{H}$	height of solid bed of polymer granules as defined in equation (2) $= H - \hat{\delta}_C - \delta_D$,
I_2	second invariant of the rate of strain tensor,
k_m, k_s	thermal conductivity of the melt, solid ($k_s = k_A$ from Parts I, II),
M_{Ax}	volume flowrate in bed A in x direction,
M_{Bx}	volume flowrate in melt pool B in x direction,
M_{Dx}, M_{Ex}	volume flowrates in zones D and E in x direction, respectively,
m_{Cz}, m_{Fz}	volume outflow in z direction per unit length in x direction in zones C and F, respectively,
M_T	total mass flux in extruder,
N	rate of revolution of the screw,
n	$= 1 - 2s$
p	isotropic pressure,
R	total volumetric melting rate at the solid–melt interfaces per unit downchannel area,
R_B, R_C, R_D, R_E	volumetric melting rates at the AB, AC, AD, and AE interfaces, respectively,
$S_{ABx}, S_{ACx}, S_{ADx}, S_{AEx}$	forces due to x shear stress on the AB, AD, AD and AE interfaces per unit downchannel distance,
s	material constant in the constitutive equation (power law index),
T	temperature,
$\bar{T}$	velocity-weighted average temperature of the melt flowing from zone C into zone B (equation 9),
T_m, T_s	temperature of molten polymer, screw, respectively,
T_0	base temperature for viscosity measurement,
v_{Ax}, v_{Ay}	velocity components of the solid bed (zone A),
v_{bx}, v_{bz}	velocity components of the barrel,
v_{Cx}, v_{Cz}	velocity components in zone C,
v_{Dx}, v_{Dz}	velocity components in zone D,
v_{Ex}	velocity component in zone E,
W	width of screw channel,
$\bar{W}$	width of melt pool as defined in equation (6) $= W - Z - \delta_E$,
W_f	width of screw flight,
x, y, z	Cartesian coordinates (downstream, radial, cross-stream),
Z	width of zone A,
β	helix angle of the screw,
$\delta_C, \delta_D, \delta_E, \delta_F$	thickness of zones C, D, E, and F,
$\hat{\delta}_C$	average thickness of zone C,
λ	latent heat of fusion,
μ	viscosity function,
ρ_m, ρ_s	density of melt, solid bed ($\rho_s = \rho_A$) from Parts I and II,
ψ_1, ψ_2	integration constants as defined in equation (14)

APPENDIX

*Description of numerical calculations**

Overall scheme. The calculations in each zone are carried out independently of each other. This approach enables the user of the program to incorporate (1) changes in the underlying assumptions and governing equations, or (2) improvements in the numerical technique employed, without changing the whole program. Use of non-dimensional groups makes it possible to use almost the same numerical scheme in zones C, D, E and F, when only the boundary conditions change and not the equations.

Calculations of the iterative scheme are carried out at three levels (see *Flowcharts 1–3*).

Level 1: The analysis steps forward from stage to stage in the downstream direction (*Flowchart 1*).

Level 2: At any one stage (i.e. at any point x), the analysis is carried out by passing through all 6 zones in the following order: Zone A (Zone B), Zone F, Zone C, Zone D, and Zone E after which it returns to Zone A for a check of convergence criteria (*Flowchart 2*).

Level 3: A predictive–corrective method is applied to solve the equations for the depth of each zone, its tempera-

* An annotated version of the melting program described above, together with full supporting documents, is available from National Research Development Corporation, P.O. Box 236, Kingsgate House, 66/74 Victoria Street, London SW1, UK, with whom the copyright resides, or from their agents, J.R.A. Pearson Engineering Consultants Ltd, 23 Chaucer Road, Cambridge CB2 2EB, England, to whom enquiries should be addressed.

ture and velocity profile (in zones *C, D, E* and *F*) or *Z*, d*p*/d*x* and v_{Ax} (in zone *A*) (*Flowcharts 3* and *4*).

Calculations at levels 1 and 2 are carried out by the main program, while level 3 calculations are executed by subroutines. The only function the program fulfils at level 1 is to calculate a new mass flow rate for zone *A*, M_{Ax}, when stepping forward in the downstream direction, i.e. *x*-direction, according to equation (3), i.e.:

$$M_{Ax}(x + \Delta x) = M_{Ax}(x) - \Delta x(R_C + R_D + R_E)$$

Here $x + \Delta x$ represents the new position while x is the position (in the downstream direction) at which calculations have just been completed. (At the first stage of the calculations we set $M_{Ax}(x) = M_T$.)

A diagram of the program at level 2 is given in *Flowchart 2*. After entering a new stage the main parameters (such as M_{Ax}, δ_C, δ_D, δ_E, d*p*/d*x*, etc.) are estimated to initialize the first cycle through the 6 zones. Zone *F* is entered first, using as input this estimated value for d*p*/d*x*. The output from zone *F* is the flowrate over the flight m_{Cz} ($z = 0$) which initializes zone *C* calculations based on finite difference analysis. The time spent in zone *F* is very short since only minor adjustments are needed because of the weak dependence of the solution on d*p*/d*x*. After zone *F* we enter zone *C*. Input for this zone is d*p*/d*x*, *Z*, v_{Ax} and m_{Cz} ($z = 0$). The channel width *W* is divided into N_z equal parts (N_z in an input variable) giving equal increments Δz in the *z*-direction. Zone *C* calculations are carried out *k* times where *k* is a positive integer with $Z \geqslant k\Delta z > Z - \Delta z$. At each point in the *z*-direction we calculate δ_C, the local melting rate m_{Cz} and the local wall stresses in the *x*-direction. The total melting rate in zone *C*, R_C, is then calculated from equation (5), i.e.:

$$R_C = m_{Cz}(z = 0) - m_{Cz}(z = Z)$$

where a linear extrapolation is applied to the difference $Z - k\Delta z$. The shear stresses for zone *C* are obtained from the local stresses by interpolation, again applying a linear extrapolation to the difference $Z - k\Delta z$. We also obtain $\hat{\delta}_C$ the mean value of the depth of zone *C* by averaging over the local values $\delta_C(z = n\Delta z)$, $0 < n \leqslant k$. Thus we obtain, as output from zone *C*, R_C, S_{ACx} and $\hat{\delta}_C$. Zone *C* calculations use the largest part of execution time of the program. After zone *C*, zone *D* is entered using d*p*/d*x*, v_{Ax}, and *Z* as input data. The output is R_D, δ_D and S_{ADx}. Finally, zone *E* is entered using d*p*/d*x*, v_{Ax} and *Z* to obtain R_E, δ_E and S_{AEx}.

If the new value of d*p*/d*x* calculated from equation (2), i.e.:

$$dp/dx = (S_{ACx} + S_{ADx} + S_{AEx})/[Z(H - \hat{\delta}_C - \delta_D)]$$

is within a certain tolerance limit of the one used during this cycle control is passed back to execution at level 1. Otherwise zone *A* is entered to obtain new values for d*p*/d*x*, v_{Ax} and *Z* using the melting rates R_C, R_D, R_E, the stresses S_{ACx}, S_{ADx} and S_{AEx}, and the depth of zones *C, D* and *E* just calculated. We now repeat this cycling through the zones starting again with zone *F* until convergence is reached.

Exceptions are: at stage number 1, *Z* is not calculated but kept constant and equal to $W - 2\delta_E$; if the screw temperature is smaller than the melting temperature zone *D* and *E* calculations are not carried out and the relevant values are set equal to zero.

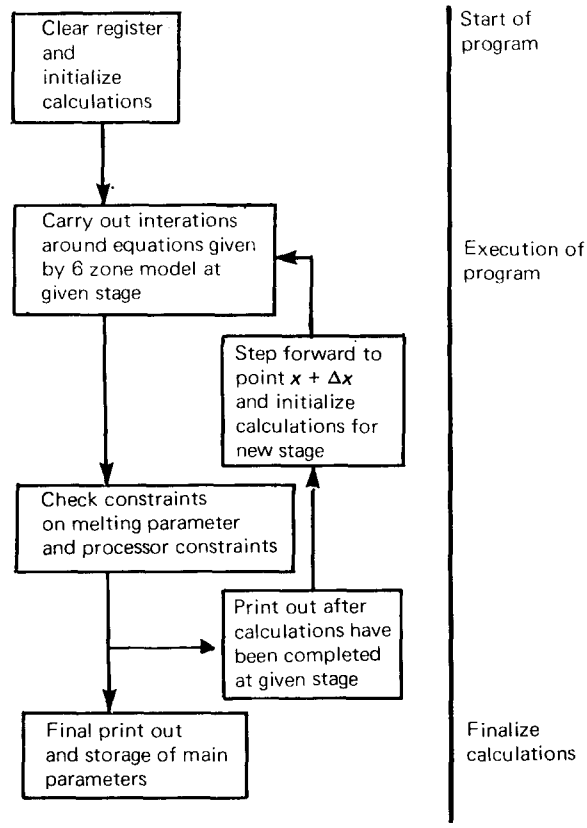

Flowchart 1 Calculations at level 1

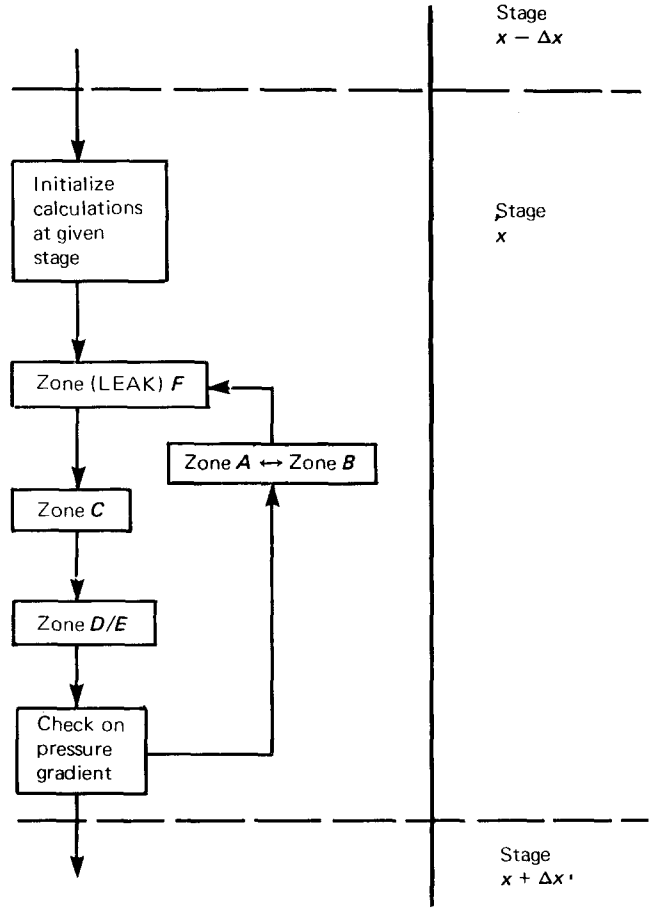

Flowchart 2 Calculations at level 2

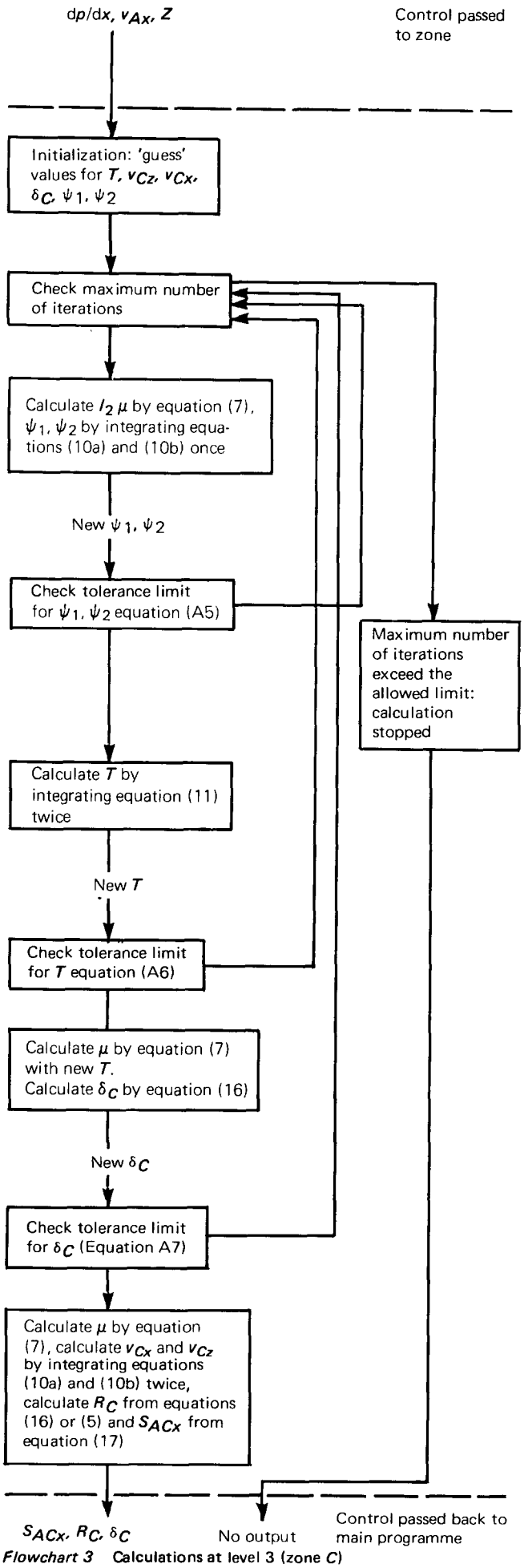

Flowchart 3 Calculations at level 3 (zone *C*)

(a) Zones *A* and *B*.

We shall start with zone *A* to describe execution at level 3, i.e. on the level of individual zones. When entering zone *A* we use as input $\hat{\delta}_C$, δ_D, δ_F, R_C, R_D, R_E, S_{ACx}, S_{ADx}, and S_{AEx} calculated in zones *C*, *D* and *E* and M_{Ax} estimated when stepping forward. We start with a guessed value for *Z* and calculate v_{Ax}, dp/dx and shear rate I_2 from:

$$v_{Ax} = M_{Ax}[Z(H - \hat{\delta}_C - \delta_D)] \quad \text{(A1)}$$

$$dp/dx = S/[Z(H - \hat{\delta}_C - \delta_D)] \quad \text{(A2)}$$

with

$$S = S_{ACx} + S_{ADx} + S_{AEx}$$

$$I_2 = \frac{1}{4}\left[\left(\frac{v_{bx}}{H}\right)^2 + \left(\frac{v_{bz}}{W}\right)^2 + \left(\frac{v_{Ax}}{\bar{W}}\right)^2\right] \quad \text{(A3)}$$

where $\bar{W} = W - Z - \delta_E$.

These are equations (4), (2) and (8), respectively. If $\bar{T}$ is the velocity-weighted average temperature of the melt flowing from zone *C* into zone *B* (i.e. equation 9) we obtain a mean viscosity given by equation (7). We then calculate the mass flowrate M_{Bx} of the melt pool according to the Rowell–Finalyson model (equation 6). If the expression:

$$\Delta M_{Ax} = (M_T - M_{Bx}\rho_m)/\rho_s - M_{Ax} \quad \text{(A4)}$$

is negative, the mass conservation equation (equation A1) is not obeyed because the mass flow in zone *A* is underestima-

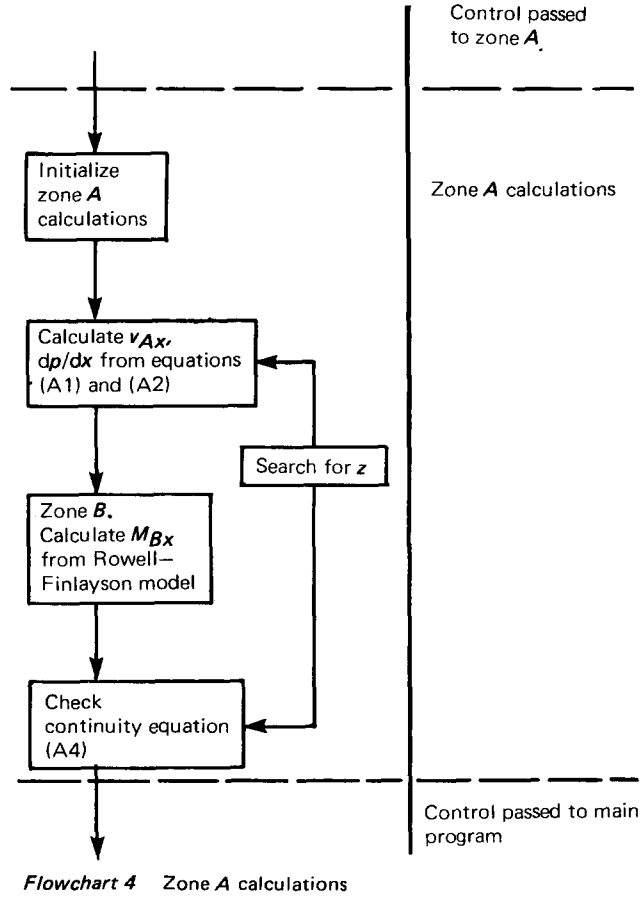

Flowchart 4 Zone *A* calculations

ted. Thus we increase Z. If ΔM_{Ax} is positive but larger than a certain tolerance limit we decrease Z thus decreasing the mass flow in zone A. This search technique converges to a value of Z for which the continuity equation holds. Now equation (1) gives v_{Ax} and equation (A2) gives a new value for dp/dx.

(b) Zone C

To complete the discussion of the execution of the program at level 3, we now consider zones C, D, E and F. The basic procedure is the same for all these zones; only the boundary conditions vary. We take zone C as an example and outline the differences for the other zones later. After initializing the calculations (see above) all variables are transformed into their non-dimensional form using the following scale factors:

$$P_{\text{scale}} = C_0(\pi D_b N)^{1-2s}/(\delta_C)^{2-2s}$$

$$\mu_{\text{scale}} = C_0(\delta_C)^{2s}/(\pi D_b N)^{2s}$$

$$T_{\text{scale}} = C_0(\pi D_b N)^{2-2s}(\delta_C)^{2s}/C_m$$

These factors are dependent on the size of zone δ_C (δ_D in zone D, δ_E in zone E) and have to be recalculated every time δ_C is calculated. Since the variables are dimensionless we do not calculate the equations given in *Flowchart 3* but their dimensionless equivalents. The exact sequence in which the equations are solved in zone C is given in *Flowchart 3*. We would like to note here only that when calculating ψ_1 and ψ_2, the first integrals of equations (10a) and (10b), respectively, we use an underestimation parameter, i.e.:

$$\psi_{1,2} = \psi'_{1,2} + P(\psi''_{1,2} - \psi'_{1,2})$$

where $\psi'_{1,2}$ is the previously calculated value while $\psi''_{1,2}$ is the value calculated from integrating equations (10a) or (10b). (A combination of Simpson's rule and Newton's 3/8 rule was used.) Empirical tests showed that $P = 1 - 2s$ optimizes the execution time for $\psi_{1,2}$ calculations. After the $\psi_{1,2}$ calculations have converged we set $\psi_{1,2} = \psi_{1,2}$.

(c) Zones D and E

When calculating δ_D or δ_E in zones D and E we again use an under-relaxation parameter to prevent overshoot of the δ_D, δ_E values. Although we enter zones D or E only once during every cycle through the zones, the calculations are extremely sensitive to changes in δ_D or δ_E since all scale factors depend on the depth of these zones.

(d) Zone F

The calculations in zone F, although two-dimensional as in zone C, are simpler than zone C, D or E calculations since its size δ_F is constant and equal to the flight gap.

(e) Boundary conditions

We now give the boundary conditions used in the zones. Note that since non-dimensionalizing is based on the depth of each zone, all variables in cross-zone directions (e.g. the y-direction in zone C) vary from 0 to 1. Calling this direction y to simplify matters for all cases, we have $y = 0$ is the melt/solid bed interface in each zone; $y = 1$ is the screw root in zone D, the screw flight in zone E, and the barrel in zone C (see *Figure 1b* for the changing use of y). Thus we have at $y = 0$:

$$v_{Cx}(y,z) = v_{Dx}(y) = v_{Ex}(y) = v_{Ax}$$

$$v_{Cz}(y,z) = v_{Fx}(y,z) = v_{Fz}(y,z) = 0$$

$$T_C(y,z) = T_D(y) = T_E(y) = T_m$$

$$T_F(y) = T_s$$

and at $y = 1$ we have:

$$v_{Cx}(y,z) = v_{Fx}(y,z) = v_{bx}$$

$$v_{Cz}(y,z) = v_{Fz}(y,z) = v_{bz}$$

$$v_{Dx}(y) = v_{Ex}(y) = 0$$

$$T_C(y,z) = T_F(y) = T_b$$

$$T_D(y) = T_E(y) = T_s$$

(f) Starting conditions

When initializing various stages of execution of the program we have to distinguish first between starting conditions for each stage (level 1 and 2 execution) and for each zone (level 3). Furthermore, the initialization is different for stage number 1 than for any subsequent stage.

The initial conditions for the first stage consist of two groups. In one group belong input data which are essential to the calculated results, i.e.: screw geometry data; polymer data; operating conditions; and initial size of zones D and E.

The second group of initial data consists of those which initialize the iterative process without affecting the final results. These are: initial pressure gradient; initial temperature and velocity profiles; initial values for integration constants; initial size of zone C.

The initial depths of zone D and E have to be specified as input data. An exteme choice can seriously affect the convergence of the numerical scheme during the first few stages. The execution time for $\delta_D = 0.01$ mm in *Figure 14* is three times as long as run 3 with $\delta_D = 0.4$ mm. The actual values of the variables belonging to the second group have no influence on the final results but will affect the speed of convergence. For this reason, initial pressure gradient and iteration constants are taken from previously converged results. Temperature and velocity profiles are set to vary linearly between the given boundary conditions, and the initial size of zone C is assumed to be

$$\delta_C(z) = \delta_F(z/1.5)^{1/2} + \delta_F$$

All other variable registers are set to zero. After the first stage has been completed the initial values for the following variables are set to the values calculated during the previous stage: size of zones; temperature and velocity profiles; and pressure gradient and integration constants. In addition, values for Z, v_{Ax} and dp/dx are linearly extrapolated after three stages have been completed, thus giving a more accurate estimate when passing through zones F, C, D and E for the first time in any new stage.

The following initialization takes place at level 3. When entering zones C, D, E or F, we start calculations with the values for size of the zone, temperature and velocity profiles and integration constants that come from the last calculated stage. Once the iterations around these values have converged these initial values are exchanged with the newly cal-

culated values. Hence the next time a zone (*C, D, E* or *F*) is entered we use more accurate initial values. An exception is zone *A*. After zone *A* has been passed more than 6 times in any one stage we use an averaged value for dp/dx when entering zone *F* instead of the calculated value. Although this means that equations (1), (2), (3) and (4) are not satisfied simultaneously by the values for v_{Ax}, Z and dp/dx used in zones *C, D, E* and *F*, the weighting of the value for dp/dx stabilizes the iterative system and thus increases the speed of convergence.

An alternative way of initializing the calculations at any new stage is the following. Before starting the calculations at any stage, the program can read from a special tape all main parameters, i.e.: size of the zone; temperature and velocity profiles; melting rates and stresses; pressure gradient, axial velocity of solid, etc. which were stored after a run with the same or slightly varying operating conditions had been completed successfully. This can be a more economic way of running a large number of jobs specifying similar operating conditions.

(g) Execution control procedure

We again distinguish between program control at three different levels (see *Flowcharts 1–4*).

At level 1 there are two different types of execution control parameters: computer dependent parameters and criteria which indicate a possible break up of solid bed. In both cases the processor is stopped and a print out of final results of the analysis is given. To the first group belong the execution time and storage space in central memory. The maximum time allowed for the execution of the program is an input variable and depends on the computer used. The storage space in the central memory is so distributed that at most 21 points can be calculated in the *x*-, *y*- or *z*-directions. If the processor stops because either time or space has run out the analysis can be continued by restarting the processor and using as input data the stored values of the last completed stage.

The second group of convergence criteria has been chosen to stabilize the iterative scheme and avoid convergence problems which occur at the end of the compression zone. This group was given the name 'break-up criteria' because experiments showed that break-up takes place at approximately the same down-channel position, and possibly even earlier. These criteria are: more than 95% of original polymer granules are molten; the size of zones *D* and *E* is larger than a given limit (here we took 3 mm for a channel depth of 3.3 mm at the end of the compression zone); the width or the depth of the solid bed is less than 10% of the channel width or channel depth; the axial velocity of the solid bed has increased by more than 50% relative to the last calculated stage or by more than 300% relative to the first stage of calculations. Although these criteria are to some extent arbitrary, they have proved to be very satisfactory during test runs of the program.

The sole criterion for stopping execution at level 2, i.e. for stepping forward in down-channel direction, consists in the requirement that the relative error between the new value for dp/dx given by (A2) and the old value, which was used in zones *C, D*, and *E* to obtain S_{ACx}, S_{ADx} and S_{AEx} is smaller than 1%.

For the calculations in zones *C, D, E* and *F* we use the following convergence criteria:

$$\left|\frac{\psi_{1,2} - \psi'_{1,2}}{\psi'_{1,2}}\right| < 0.1\% \qquad \text{(A5)}$$

where $\psi'_{1,2}$ is the previous value for the integration constant ψ_1 or ψ_2:

$$\sum_y \left|\frac{T(y) - T'(y)}{T'(y)}\right| < 0.1\% \qquad \text{(A6)}$$

where T' is the previous temperature profile; and finally

$$\left|\frac{\delta_I - \delta'_I}{\delta'_I}\right| < 0.1\% \qquad \text{(A7)}$$

where δ'_I is the previously calculated value and $I = C, D,$ or *E*. The maximum number of iterations permitted for any one loop (i.e. for $\psi_{1,2}$, T, or δ calculations) is 200, after which the program stops and non-convergence is assumed. The maximum number for dp/dx iterations is 20, i.e. if all zones have been passed 20 times at any one stage we again assume non-convergence of the iterative scheme and the processor is stopped.